P1D.7

Interpreting Dropsonde Measurements of Turbulence in the Tropical Cyclone Boundary Layer

Jeffrey D. Kepert *
Centre for Australian Weather and Climate Research
A partnership between the Australian Bureau of Meteorology and CSIRO

AMS Hurricanes Conference, Apr 28 - May 2, 2008

1. Introduction

Some of the most dangerous winds on earth occur in tropical cyclones. Their destructive power depends as much on their gustiness, or turbulence, as on their mean strength. Further, the efficiency with which energy is extracted from the ocean to power the tropical cyclone depends strongly on the boundary layer turbulence. Thus understanding turbulence in the tropical cyclone boundary layer is crucial. At one level, this understanding should be a simple problem because stability effects become small as the wind speed increases. At another, the problem is complex because the strong winds severely modify the air-sea interface. Finally, testing theoretical predictions and extrapolations from lower wind speeds is problematic due to the severe difficulty in taking observations where it matters, in close to the interface.

Over the last decade, U.S. hurricane reconnaissance aircraft have deployed thousands of dropsondes in and near the eyewall of tropical cyclones. These instruments parachute towards the surface, reporting back wind, temperature, humidity and pressure at $\frac{1}{2}$-second intervals, or about every 6 m vertically (Hock and Franklin 1999). These measurements have had a considerable impact on our knowledge of the mean structure of the tropical cyclone boundary layer (Franklin et al. 2003; Wroe and Barnes 2003; Schneider and Barnes 2005; Kepert 2006a,b; Montgomery et al. 2006; Bell and Montgomery 2008; Schwendike and Kepert 2008), but the high sampling rate implies that there is a considerable potential to illuminate the turbulent structure as well. Figure 1 shows the hodograph of a single dropsonde deployed into the eyewall of Hurricane Georges (1998). It is clear that the measured wind profile is consistent with many of the characteristics of turbulence: it is random, spatially correlated, contains multiple scales, and is vortical.

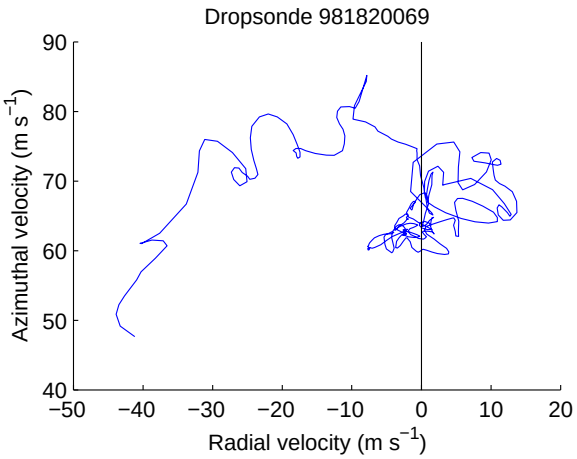

Fig. 1. Measured wind hodograph from a dropsonde deployed into the eyewall of Hurricane Georges on 19 September 1998.

This paper presents a theoretical frame-

*Centre for Australian Weather and Climate Research, Bureau of Meteorology, 700 Collins St, Melbourne Vic 3000. Email: J.Kepert@bom.gov.au

work for interpreting the turbulence signal within these measurements. Proper interpretation requires close attention to the response characteristics of the instrument, careful quality control, and a suitable theoretical description of 3-dimensional surface layer turbulence.

Several useful results can be inferred from the comparison of theory and measurement. This paper will focus on one of these, the marine drag coefficient C_D. The main result is that C_D does not increase indefinitely with wind speed, thus confirming recent direct measurements (Powell et al. 2003; Black et al. 2007; French et al. 2007) by a new and independent technique, and extending those results to much higher wind speeds.

2. Theory

a. Air-sea momentum exchange

The surface stress τ may be written

$$\tau = \rho C_D U_{10}^2 = \rho u_*^2 \tag{1}$$

where ρ is the air density, U_{10} is the 10-m mean wind speed and C_D the drag coefficient. Over the ocean, C_D is thought to increase approx linearly with wind speed, as reflected in numerous empirical parameterisations, for example Large and Pond (1981). The drag coefficient can be related to the surface roughness length z_0 through the logarithmic wind profile,

$$U(z) = \frac{u_*}{k} \log\left(\frac{z}{z_0}\right) \tag{2}$$

with $z = 10$ m, where k is von Kärmän's constant and the roughness length z_0 over the ocean is frequently parameterised after Charnock (1955)

$$z_0 = \alpha \frac{u_*^2}{g}. \tag{3}$$

Here α, the Charnock coefficient, is an empirical constant and g is the gravitational acceleration. The value $\alpha = 0.011$ is widely used, see for example Fairall et al. (2003). Charnock's relation (3) in combination with (1) and (2) is quite consistent with a linear increase of C_D over the wind speed range of interest.

b. Dropsonde dynamics

In this section, a theory is developed for the mean and turbulent accelerations experienced by a dropsonde as it falls through the atmospheric surface layer. The turbulent part of the theory is an extension of Kristensen (1993)'s analysis of cup anemometer dynamics to the case where the mean flow and the turbulence are not stationary in time.

The dropsonde is a first-order linear filter of the true wind (Hock and Franklin 1999):

$$\tilde{u}(t) = \tilde{s}_x(t) + \tau_0 \dot{\tilde{s}}_x(t) \tag{4}$$

where $(\tilde{u}, \tilde{v})$ is the instantaneous horizontal wind vector, $(\tilde{s}_x, \tilde{s}_y)$ is the horizontal component of the dropsonde velocity, $\tau_0 = v_f/g \approx 1.2$ s is a time scale, and v_f is the dropsonde fall velocity. We adopt the usual surface-layer convention that the x-axis is in the mean wind direction, y is to the left and z is upwards. The solution of (4) is (Kristensen 1993)

$$\tilde{s}_x(t) = \frac{1}{\tau_0} \int_0^\infty e^{-\tau/\tau_0} \tilde{u}(t-\tau) d\tau \tag{5}$$

We decompose all variables into mean and fluctuating components, $\tilde{u}(t) = U(t) + u(t)$, $\tilde{s_x}(t) = S_x(t) + s_x(t)$,

$$U(t) = S_x(t) + \tau_0 \dot{S}_x(t) \tag{6}$$

$$u(t) = s_x(t) + \tau_0 \dot{s}_x(t) \tag{7}$$

Here, the ergodic hypothesis is unavailable because the dropsondes are falling through gradients of both mean and turbulence quantities, and so "mean" should be interpreted as an ensemble-average following the dropsonde trajectory.

In the case where the mean wind profile $U(z)$ is logarithmic (2), an analytic solution is available for (6),

$$S_x(t) = U(t) - \frac{u_*}{k} e^{-t/\tau_0} \mathrm{Ei}\left(\frac{t}{\tau_0}\right), \tag{8}$$

where Ei is the exponential integral function and the dropsonde fall velocity has been used for the space-time conversion, $t = -v_f z$.

An expression for the variance of the dropsonde acceleration is found by multiplying (7) in turn by u, s_x and $\dot{s}_x$, ensemble-averaging, and a little manipulation

$$\langle \dot{s_x}^2 \rangle = \frac{\langle u^2 \rangle - 2\langle u s_x \rangle + \langle s_x^2 \rangle}{\tau_0^2} \tag{9}$$

Angle brackets denote an ensemble average at any fixed point in the dropsonde trajectory. We now proceed to evaluate the right-hand side of (9).

Taking the fluctuating part of (5), multiplying by u and ensemble-averaging,

$$\langle u s_x \rangle = \int_0^\infty R_u(-\tau) e^{-\tau/\tau_0} d(\tau/\tau_0), \tag{10}$$

where

$$R_u(-\tau) = \langle u(t) u(t-\tau) \rangle \tag{11}$$

is the autocovariance of the along-stream wind component with lag $-\tau$. We represent R_u by its spectrum S_u,

$$R_u(-\tau) = \int_{-\infty}^\infty S_u(f) e^{-2\pi i f \tau} df \tag{12}$$

Thus the covariance between the x-component of the dropsonde and wind velocities is

$$\langle u s_x \rangle = \int_{-\infty}^\infty \frac{1}{1 + 4\pi^2 f^2 \tau_0^2} S_u(f) df \tag{13}$$

Note that the wind velocity variance can also be written in terms of S_u by virtue of Parseval's theorem,

$$\langle u^2 \rangle = \int_{-\infty}^\infty S_u(f) df \tag{14}$$

Multiplying (7) by s_x and ensemble-averaging gives another equation for a first-order linear filter,

$$\langle u s_x \rangle = \langle s_x^2 \rangle + \tau_0 \langle s_x \dot{s_x} \rangle = \langle s_x^2 \rangle + \frac{\tau_0}{2} \frac{\partial \langle s_x^2 \rangle}{\partial t}, \tag{15}$$

With initial condition $\langle s_x^2(-\infty) \rangle = 0$, the solution is

$$\langle s_x^2(t) \rangle = \frac{2}{\tau_0} \int_0^\infty e^{-2\tau/\tau_0} \langle u(t-\tau) s_x(t-\tau) \rangle d\tau \tag{16}$$

which can be evaluated from (13) by a numerical integration.

Note that

$$\langle u^2 \rangle - \langle u s_x \rangle = \int_{-\infty}^\infty \frac{4\pi^2 f^2 \tau_0^2}{1 + 4\pi^2 f^2 \tau_0^2} S_u(f) df = \mathcal{H}_u \tag{17}$$

and

$$\langle s_x^2 \rangle - \langle u s_x \rangle = \mathcal{H}_u - \frac{2}{\tau_0} \int_0^\infty \mathcal{H}_u e^{-2\tau/\tau_0} d\tau \tag{18}$$

where $\mathcal{H}_u$ is a high-pass filtered wind velocity variance. Thus, from (9) the dropsonde x-acceleration variance $\langle \dot{s_x}^2 \rangle$ depends only on the high-frequency part of the turbulence spectrum, consistent with the fact that differentiation is a high-pass filtering operation.

Dropsondes do not measure a simultaneous wind profile, but rather a time-series along a slant trajectory. Thus the above theory requires the autocorrelation of the time-series along the dropsonde slant trajectory:

$$\begin{aligned} R_u(-\tau) &\equiv R_u(-U\tau, 0, v_f\tau, -\tau) \\ &= R_u(0, 0, v_f\tau, 0), \end{aligned} \tag{19}$$

where the equality with the instantaneous vertical profile follows by Taylor's hypothesis.

Thus the one-dimensional line spectrum in the vertical direction, $F_{11}^3(k_3)$, is required. There seem to be no published forms for such spectra in the atmospheric surface layer, but they may be derived from the full spectral velocity tensor, theoretical forms of which were given by Kristensen et al. (1989) and Mann (1994). Here, we shall adopt the former.

The one-dimensional along-stream turbulence line spectrum is defined as the Fourier

transform of the along-stream autocorrelation

$$F_{ij}^1(k_1) = \frac{1}{2\pi}\int_{-\infty}^{\infty} e^{-ik_1 r_1} R_{ij}^1(r_1) dr_1 \qquad (20)$$

where the indices $i, j = 1, 2, 3$ refer to the three Cartesian axes. The spectral tensor is the extension of this transformation to three dimensions,

$$\Phi_{ij}(\mathbf{k}) = \frac{1}{(2\pi)^3}\iiint_{\mathbb{R}^3} R_{ij}(\mathbf{r}) e^{-i\mathbf{k}\cdot\mathbf{r}} d\mathbf{r} \qquad (21)$$

Line spectra in any direction may be obtained from $\Phi_{ij}(\mathbf{k})$ by integrating out the components of $\mathbf{k}$ normal to the desired direction. In particular, vertical line spectra are obtained by

$$F_{ij}^3(k_3) = \int_{-\infty}^{\infty}\int_{-\infty}^{\infty} \Phi_{ij}(k_1, k_2, k_3) dk_1 dk_2 \qquad (22)$$

Figure 2 shows the variance vertical line-spectra F_{11}^3 (along-stream), F_{22}^3 (cross-stream) and F_{33}^3 (vertical) so found, compared to the well-known along-stream line-spectra of Kaimal et al. (1972). The differences include the expected 4/3 ratios in the inertial subrange.

Velocity differences a in turbulence over small time or space scales have a probability density function (PDF) (Castaing et al. 1990)

$$p(a) = \int_0^{\infty} \frac{1}{2\pi\lambda\sigma^2} e^{-a^2/(2\sigma^2)} e^{-\log(\sigma/\sigma_0)^2/(2\lambda^2)} d\sigma \qquad (23)$$

This distribution is equivalent to drawing data from an infinite ensemble of Gaussian distributions with mean 0 and variance σ^2, where $\log(\sigma)$ is drawn from a Gaussian with mean $\log(\sigma_0)$ and variance λ^2. It has "fatter tails" than a Gaussian, and has been shown to fit laboratory (Castaing et al. 1990) and atmospheric (Boettcher et al. 2003) turbulence data well. We found that $\lambda = 0.6$ gave a good fit to tropical cyclone dropsonde data. An example is shown in Fig 3, where

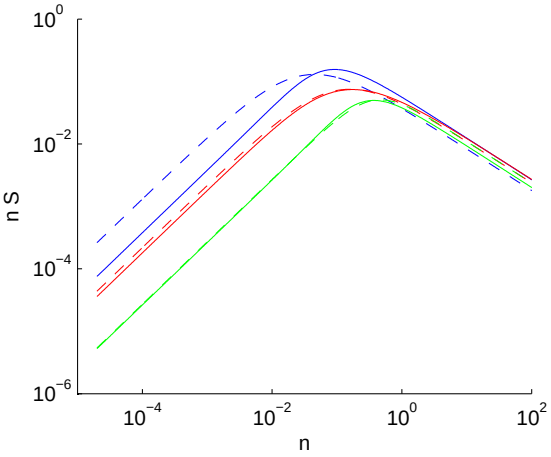

Fig. 2. Atmospheric surface-layer velocity line spectra, for the u (blue), v (red) and w (green) velocity components. The dashed curves are for line spectra in the along-stream direction, and the solid curves are for the vertical.

the excellent fit of (23) to the observed PDF is apparent, along with it's superiority to a Gaussian. The fit is slightly less successful for the vertical component of acceleration, probably due to an unequal dropsonde response to upwards and downwards turbulent fluctuations leading to a slight skewing of the observed distribution.

In summary, this theory allows us to calculate the dropsonde acceleration variance due to turbulence within the atmospheric surface layer, as a function of height and friction velocity only. The theory has been presented for the x-component of acceleration variance, with the main changes for the y-component being that the mean acceleration is 0 instead of (8) and the use of the appropriate spectrum. Given these variances and the empirical $\lambda = 0.6$, Castaing et al.'s distribution then allows calculation of the PDF of the acceleration components due to turbulence. The dropsonde will also experience an acceleration due to its falling through a sheared mean flow, given by differentiating (8). Combining the mean and turbulent components gives the PDF of the

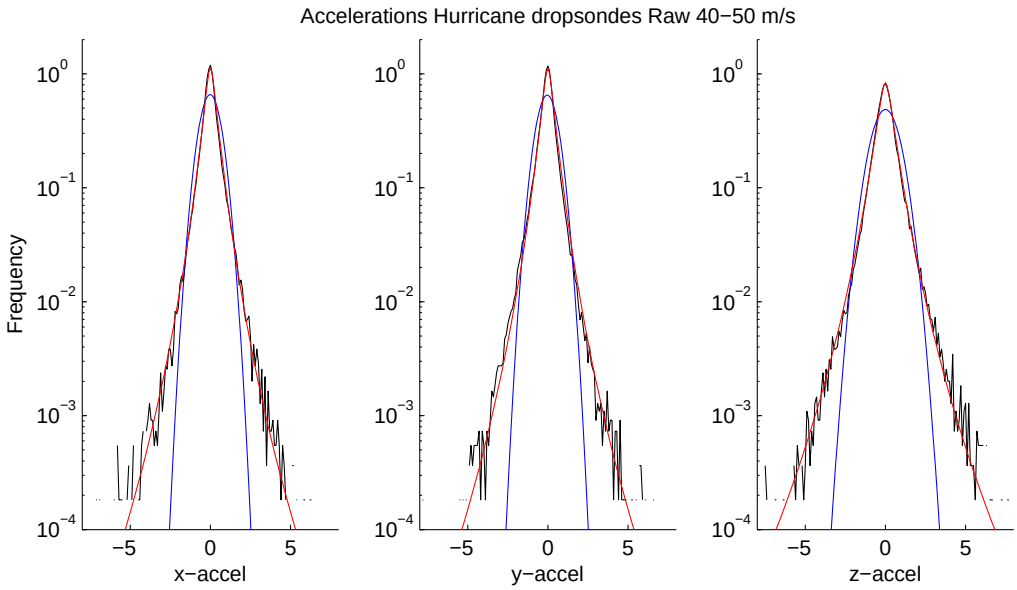

Fig. 3. Comparison of acceleration PDF's. Black curves: Observed acceleration from dropsondes at all heights and with BLM wind speeds in the range of 30 – 40 m s^{-1}. Blue curves: Gaussian with the observational variance. Red curves: Castaing et al.'s PDF (23) with $\lambda = 0.6$ and the observational variance. In this figure only, the x-axis is oriented eastwards rather than in the mean flow direction.

total acceleration over the layer, which will be compared to observations below. These theoretical calculations were performed using a Monte Carlo technique for a range of friction velocities and 10-m wind speeds, and the acceleration PDFs accumulated over depths 0 – 50 m, 0 – 100 m and 0 – 150 m.

3. Observations

The GPS dropsonde has been described by Hock and Franklin (1999). The filtering of the true wind by the inertia of the instrument has been taken into account by the above theory; thus we use raw soundings with no motion correction and no filtering applied. The profiles are subjected to quality control checks for fall velocity consistency between GPS and pressure measurements, and for valid splash point and launch detection. The soundings are stratified into 10 m s^{-1}-wide bins according to the mean wind speed below 600-m height (the boundary layer mean, BLM), as in Powell et al. (2003). The mean wind direction is calculated over the lowest 100 m before splash, and the three acceleration components in that reference frame are calculated by finite differences. Histograms of acceleration frequency are accumulated in 0.1 m s^{-2}-wide bins over the same height ranges as for the theoretical calculation. To date, all 5248 available dropsondes up to the end of the 2002 hurricane season have been processed.

4. Results

a. Comparison to Charnock (1955)

Figure 4 displays the theoretical and observed horizontal acceleration PDFs when u_* is calculated from the 10-m mean wind speed using Charnock's relation (3) with coefficient 0.011 (Fairall et al. 2003). For BLM wind speeds below 30 m s^{-1} (10-m mean wind up to about 23 m s^{-1}, the upper two panels), excellent agreement is obtained be-

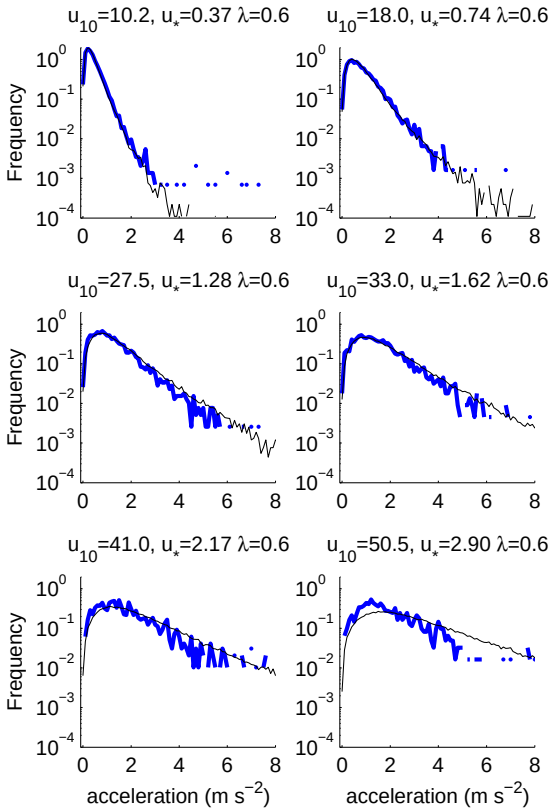

Fig. 4. Theoretical (black) and observed (blue) PDFs of dropsonde acceleration in the lowest 100 m of the atmosphere. The BLM wind speed ranges are, from top left, 10 – 20 m s^{-1}, 20 – 30 m s^{-1}, 30 – 40 m s^{-1}, 40 – 50 m s^{-1}, 50 – 60 m s^{-1}, and over 60 m s^{-1}. The observed mean 10-m wind speeds are as shown, together with friction velocities calculated using Charnock's formula.

tween theory and observations. As surface momentum transfer is generally believed to be well-understood in this wind speed range, this agreement provides confirmation of the validity of the method.

As the BLM wind speed increases, a discrepancy between theory and observations appears and grows. Relative to the theory, high accelerations are too rarely, and low accelerations too commonly, observed. Dropsondes tend to fail near the surface at high wind speeds (Franklin et al. 2003; Powell et al. 2003), possibly due to a failure of the GPS sensor to maintain synchronisation with the satellite under extreme acceleration. The paucity of high accelerations observed could be due to this failure; however, if the failures were due to this reason alone then the relative gap between the theoretical and observed curves in Fig 4 would be the same at any given acceleration in all panels. This is not so, so we conclude that dropsonde failure is not the dominant reason for the poor agreement.

Rather, the paucity of high accelerations is accompanied by an abundance of low ones. Reducing the surface roughness in the theoretical calculation would lead to a decrease in the turbulence intensity and hence in the relative frequency of high accelerations. Hence we conclude that Charnock's relation, within the theory presented here, overestimates the marine surface roughness at extreme wind speeds.

Similar results were obtained when Large and Pond (1981)'s parameterisation of C_D was used in place of Charnock's relation.

b. Comparison to Powell et al. (2003)

Figure 5 shows a similar comparison to Fig. 4, except that the roughness lengths derived by Powell et al. (2003) are used. Excellent agreement is obtained between theory and observation. We thus conclude, subject to the limitations of the dropsonde acceleration theory, that Powell et al. (2003)'s roughness lengths are consistent with the observations of dropsonde acceleration.

Estimating error bars in a complex calcu-

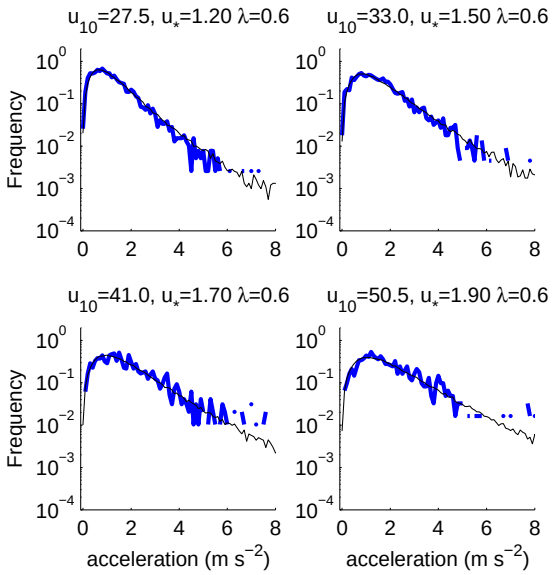

Fig. 5. As for Fig. 4 except for the highest four wind speed ranges only, and using the roughness lengths obtained by Powell et al. (2003) in place of Charnock's.

lation such as this is difficult and has not yet been attempted. However, increasing u_* by 10% significantly degrades the agreement in Fig. 5 (not shown). Given that $C_D = (u_*/U_{10})^2$, we therefore argue that drag coefficients derived from these u_* values are accurate to within 20% or better.

5. Conclusions

We have developed a theory, with free parameters u_* and u_{10}, for the mean and turbulent accelerations experienced by a dropsonde as it falls through the atmospheric surface layer. These free parameters may be adjusted to fit the theory to observations, and crucial air-sea exchange parameters such as the roughness length and drag coefficient thereby derived.

The results show that the widely-used Charnock relation, and similar empirical parameterisations of C_D such as Large and Pond (1981), lead to a prediction at extreme wind speeds of overly frequent high accelerations and insufficient low ones, in comparison to the observations. In contrast, the drag coefficients determined by Powell et al. (2003) produce excellent agreement between theory and observations.

Note that the method presented here uses a completely different part of the dropsonde signal to Powell et al. (2003), who fit logarithmic profiles to the data, thereby effectively applying a low-pass filter. In contrast, we differentiate the profile to obtain the acceleration, a high-pass filtering operation.

These results should be regarded as preliminary. Work is ongoing to

- process dropsonde data from 2003 onwards,
- use narrower velocity bins,
- perform statistical significance testing,
- compare results using the spectral velocity tensor of Mann (1994) in place of that of Kristensen et al. (1989), and
- consider along-stream and cross-stream acceleration components separately.

These results will be reported in due course.

Nevertheless, these preliminary results confirm earlier studies. The marine drag coefficient does not increase indefinitely with wind speed in tropical cyclones, but rather reaches a maximum at a 10-m wind speed in the vicinity of 30 – 35 m s^{-1}. This confirmation is independent of earlier studies that produced a similar result, as it uses a different part of the data and relies upon a novel and independent technique.

6. Acknowledgement

I am immensely grateful to the NOAA Hurricane Research Division for making the dropsonde data available that was used in this research.

References

Bell, M. M. and M. T. Montgomery, 2008: Observed structure, evolution and potential

intensity of category five Hurricane Isabel (2003) from 12 - 14 September. *Mon. Wea. Rev.*, in press.

Black, P. G., E. A. D'Asaro, W. M. Drennan, J. R. French, P. P. Niiler, T. B. Sanford, E. J. Terrill, E. J. Walsh, and J. A. Zhang, 2007: Air–sea exchange in hurricanes: Synthesis of observations from the coupled boundary layer air–sea transfer experiment. *Bull. Amer. Meteor. Soc.*, **88**, 357–374.

Boettcher, F., C. H. Renner, H.-P. Waldl, and J. Peinke, 2003: On the statistics of wind gusts. *Boundary-Layer Meteor.*, **108**, 163–173.

Castaing, B., Y. Gagne, and E. J. Hopfinger, 1990: Velocity probability density functions of high Reynolds number turbulence. *Physica D*, **46**, 177–200.

Charnock, H., 1955: Wind stress on a water surface. *Quart. J. Roy. Meteor. Soc.*, **81**, 639–640.

Fairall, C. W., E. F. Bradley, J. E. Hare, A. A. Grachev, and J. B. Edson, 2003: Bulk parameterization of air-sea fluxes: Updates and verifications for the coare algorithm. *J. Clim.*, **16**, 571–591.

Franklin, J. L., M. L. Black, and K. Valde, 2003: GPS dropwindsonde wind profiles in hurricanes and their operational implications. *Wea. and Forecasting*, **18**, 32–44.

French, J. R., W. M. Drennan, J. A. Zhang, and P. G. Black, 2007: Turbulent fluxes in the hurricane boundary layer. Part I: Momentum flux. *J. Atmos. Sci.*, **64**, 1089–1102.

Hock, T. F. and J. L. Franklin, 1999: The NCAR GPS dropwindsonde. *Bull. Amer. Meteor. Soc.*, **80**, 407–420.

Kaimal, J. C., J. C. Wyngaard, Y. Izumi, and O. Cote, 1972: Spectral characteristics of surface-layer turbulence. *Quart. J. R. Meteorol. Soc.*, **98**, 563–589.

Kepert, J. D., 2006a: Observed boundary–layer wind structure and balance in the hurricane core. Part I: Hurricane Georges. *J. Atmos. Sci.*, **63**, 2169–2193.

———, 2006b: Observed boundary–layer wind structure and balance in the hurricane core. Part II: Hurricane Mitch. *J. Atmos. Sci.*, **63**, 2194–2211.

Kristensen, L., 1993: The Cup Anemometer, and Other Exciting Instruments. Risø report r-615(en), Risø National Laboratory, Roskilde, Denmark.

Kristensen, L., D. H. Lenschow, P. Kirkegaard, and M. Courtney, 1989: The spectral velocity tensor for boundary-layer turbulence. *Boundary-Layer Meteorol.*, **47**, 149–193.

Large, W. G. and S. Pond, 1981: Open ocean momentum flux measurements in moderate to strong winds. *J. Phys. Oceanogr.*, **11**, 324–336.

Mann, J., 1994: The spatial structure of neutral atmospheric surface-layer turbulence. *J. Fluid Mech.*, **273**, 141–168.

Montgomery, M. T., M. M. Bell, S. D. Aberson, and M. L. Black, 2006: Hurricane Isabel (2003): New insights into the physics of intense storms. Part I. *Bull. Amer. Meteor. Soc.*, **86**, 1335–1347.

Powell, M. D., P. J. Vickery, and T. A. Reinhold, 2003: Reduced drag coefficient for high wind speeds in tropical cyclones. *Nature*, **422**, 279–283.

Schneider, R. S. and G. M. Barnes, 2005: Low-level thermodynamic, kinematic, and reflectivity fields of hurricane bonnie (1998) at landfall. *Mon. Wea. Rev.*, **133**, 3243–3259.

Schwendike, J. and J. D. Kepert, 2008: The boundary–layer winds in Hurricanes Danielle (1998) and Isabel (2003). *Mon. Wea. Rev.*, **136**, in press.

Wroe, D. R. and G. M. Barnes, 2003: Inflow layer energetics of Hurricane Bonnie (1998) near landfall. *Mon. Wea. Rev.*, **131**, 1600–1612.